

# Exploration of Quantum Computer Power Side-Channels

Chuanqi Xu  
Yale University  
New Haven, CT, USA  
chuanqi.xu@yale.edu

Ferhat Erata  
Yale University  
New Haven, CT, USA  
ferhat.erata@yale.edu

Jakub Szefer  
Yale University  
New Haven, CT, USA  
jakub.szefer@yale.edu

## ABSTRACT

Noisy Intermediate-Scale Quantum (NISQ) quantum computers are being rapidly improved, with bigger numbers of qubits and improved fidelity. The rapidly increasing qubit counts and improving the fidelity of quantum computers will enable novel algorithms to be executed on the quantum computers, and generate novel results and data whose intellectual property will be a highly-guarded secret. At the same time, quantum computers are likely to remain specialized machines, and many will be controlled and maintained in a remote, cloud-based environment where end users who want to come up with novel algorithms have no control over the physical space. Lack of physical control by users means that physical attacks could be possible, by malicious insiders in the data center, for example. This work shows for the first time that power-based side-channel attacks could be deployed against quantum computers. The attacks could be used to recover information about the control pulses sent to quantum computers. From the control pulses, the gate level description of the circuits, and eventually the secret algorithms can be reverse engineered. This work demonstrates how and what information could be recovered, and then in turn how to defend from power-based side-channels. Real control pulse information from real quantum computers is used to demonstrate potential power-based side-channel attacks. Meanwhile, proposed defenses can be deployed already today, without hardware changes.

## 1 INTRODUCTION

Quantum computers have gained more and more attention, especially as large numbers of quantum computers are easily accessible over the internet. Due to the expensive nature of the quantum computing equipment, these computers are currently available as cloud-based systems. Cloud-based services such as IBM Quantum [26], Amazon Bracket [5], and Microsoft Azure [35] already provide access to various types of Noisy Intermediate-Scale Quantum (NISQ) from different vendors. Remote access makes it easy for different users and companies to run algorithms on real quantum computers without the need to purchase or maintain them. On the other hand, the users have no control over the physical space where the quantum computers are. While the cloud providers may not be bad actors themselves, the threat of malicious insiders within data centers or cloud computing facilities is well-known in classical security. These malicious insiders may have physical access to the equipment of quantum computers.

Separately, a large number of companies and startups are working on the development of quantum algorithms. These companies or startups do not themselves have quantum computers, but depend on remote access to real machines from the cloud providers. They can use a convenient pay-per-use model to run circuits on real

quantum computers. However, given possibly important intellectual property being developed by companies and startups, there is a need to understand if and how sensitive information could be extracted from the operational behavior of quantum computers. Without physical control of the machines, their circuits may be subject to side-channel attacks, even without the knowledge of these companies or startups.

### 1.1 From Classical to Quantum Computer Side-Channel Attacks

In classical computers, side-channels of different types are a well-known threat [46]. Among the side-channels there are timing- and power-based channels, which are major categories of side-channels that have been researched. There are also thermal, EM, acoustic, and a variety of other categories of side-channels. Timing side-channels are easier to exploit as they only require timing measurement of the victim to be done. Power side-channels are more powerful, but require physical access. With physical access, malicious insiders or other attackers can get detailed information about the execution of the target computer. In classical computers, there are even existing platforms for exploiting and researching power-side channels. Meanwhile, prior to this work, there has not been an exploration of power-side channels in real quantum computers.

In quantum computers, directly copying the quantum states is not possible due to the no-cloning theorem. The no-cloning theorem states that it is impossible to create an independent and identical copy of an arbitrary unknown quantum state [18, 39, 52]. However, there is no such limitation on the classical control operations performed on quantum computers. Quantum computers, such as superconducting qubit machines from IBM, Rigetti, or others, use RF pulses to “execute” gate operations on single qubits or two-qubit pairs. The control pulses are fully classical and could be spied on. Given control pulse information, as this work shows, it is possible to reverse engineer the sequence of quantum gates executed on the quantum computer. From the sequence of gates, the algorithm executed can be recovered. As this work shows, anybody with access to power measurements of the control pulse generation logic can capture and recover the control information. While this work explores power-based side-channels, the same or similar ideas could apply to EM or other types of physical side-channels. This is left as future work.

### 1.2 Power-Side Channel Threats to Quantum Computers

This work explores a number of new physical security issues in quantum computers. As these computers are currently, mostly cloud-based, without the user’s control over the physical environment, even if the cloud provider is trusted or has no business

incentive to spy on users, malicious insiders or other attackers could be motivated to use side-channels to extract information about algorithms executed on these computers.

Figure 1b shows the operation of today’s cloud-based quantum computers. Remote users submit jobs to the cloud provider, where the job management or similar server dispatches the jobs to particular quantum computers, also called backends on IBM Quantum. Typically the digital instructions are sent to controller logic, such as microwave electronics, which generate the actual control signals sent to the quantum computer.

In this work, we focus on and demonstrate potential new, side-channels used to extract information about user circuits, i.e., quantum programs. Rather than target the superconducting qubits themselves (which are isolated in a cryogenic refrigerator), we focus on the controller electronics shown in the middle of Figure 1b.

We note that in the threat model, discussed in more detail in Section 3, we assume that the classical computer components, e.g., the job management server, are protected from side-channels. There is a large body of research on the protection of classical computers from power side-channels, e.g., [1, 3, 6–8, 11, 19, 37, 41, 49, 50]. Meanwhile, controller electronics of quantum computers have not been analyzed for potential side-channels before this work.

### 1.3 Attacker’s Goals

The focus of this work is to demonstrate that it can be possible to recover various information about user circuits, i.e., quantum programs, from side-channel information. We present different types of possible information that can be recovered:

- (UC) **User Circuit Identification** – Given knowledge about the set of possible circuits executed on the quantum computer, find which circuits the user actually executed.
- (CO) **Circuit Oracle Identification** – Given a known circuit, such as Bernstein-Vazirani [9], but an unknown oracle, find the configuration of the oracle used in that circuit.
- (CA) **Circuit Ansatz Identification** – Given a known circuit, such as a variational circuit used in machine learning applications [40], but an unknown ansatz, find the configuration of the ansatz used in that circuit.
- (QM) **Qubit Mapping Identification** – Given a known circuit, identify the placement of which physical qubits were used.
- (QP) **Quantum Processor Identification** – Given knowledge about the pulses for quantum processors and a circuit, find the quantum processor on which the circuit was executed.
- (RP) **Reconstruction from Power Traces** – Given knowledge about the pulses for quantum computer basis gates, reconstruct the complete, unknown circuit from the power traces.

### 1.4 Types of Attacks

Considering the attacker’s physical access to the quantum computers, this work demonstrates various types of attacks that can be used to recover the above information.

**Timing Attack** – While this work mainly focuses on power side-channels, we start off by demonstrating simple timing side-channels to help recover user circuits (UC). The limitation of this attack also motivates work on power side-channels attacks.

**Single Measurement Attacks** – We next demonstrate single measurement attacks by showing that total energy data and average power data can be used to recover users’ circuits (UC) as well. This can also be applied to other attacker’s goals we listed in the previous section.

**Total Power Single Trace Attacks** – Considering a restricted scenario where the attacker does not access each channel, but instead measures a trace of the total power of all the channels, the attacker can recover user circuits (UC), circuit oracle (CO), circuit ansatz (CA), qubit mapping (QM), and quantum processor (QP) with some accuracy.

**Per-Channel Single Trace Attacks** – We present attacks that collect power traces from drive and control channels. There are unique drive and control channels, on which microwave pulses are sent, for each single qubit gate and multi-qubit gate. We show that attackers can collect power traces of these channels to perform reconstruction from power traces (RP), thus recovering user circuits.

## 1.5 Paper Organization

The remainder of the paper is organized as follows:

- Background on quantum computation is given in Section 2.
- The threat model is provided in Section 3.
- Experimental setup is discussed in Section 4.
- Evaluation of the attacks is in Section 5.
- Defenses are discussed in Section 6.
- The paper concludes in Section 7.

## 2 BACKGROUND

This section provides background on quantum computers and typical quantum computer workflow.

### 2.1 Qubits and Quantum States

The quantum bit, or qubit for short, is the most fundamental building block of quantum computing and is conceptually similar to the bit in present classical computing. A qubit, analogous to a bit, has two basis states, denoted by the bra-ket notation as  $|0\rangle$  and  $|1\rangle$ . However, a qubit can be any linear combination of  $|0\rangle$  and  $|1\rangle$  with norm 1, but a classical bit can only be either 0 or 1. Generally, a qubit  $|\psi\rangle$  is more specifically represented as:

$$|\psi\rangle = \alpha |0\rangle + \beta |1\rangle,$$

where  $\alpha$  and  $\beta$  are complex numbers satisfying  $|\alpha|^2 + |\beta|^2 = 1$ .

It is common to denote qubits using vector representation. The basis states for one qubit can be expressed as two-dimensional vectors, for example,  $|0\rangle = [1, 0]^T$  and  $|1\rangle = [0, 1]^T$ . As a result, the state  $|\psi\rangle$  above can be written as  $|\psi\rangle = \alpha |0\rangle + \beta |1\rangle = [\alpha, \beta]^T$ . For multi-qubit states, similar representations exist. For instance, the four basis states  $|00\rangle$ ,  $|01\rangle$ ,  $|10\rangle$ , and  $|11\rangle$  make up the space on which two-qubit states live. More generally, there are  $2^n$  basis states in the space of  $n$ -qubit states, ranging from  $|0 \dots 0\rangle$  to  $|1 \dots 1\rangle$ , and a  $n$ -qubit state  $|\phi\rangle$  can be expressed by:

$$|\phi\rangle = \sum_{i=0}^{2^n-1} a_i |i\rangle$$

where  $\sum_{i=0}^{2^n-1} |a_i|^2 = 1$ .

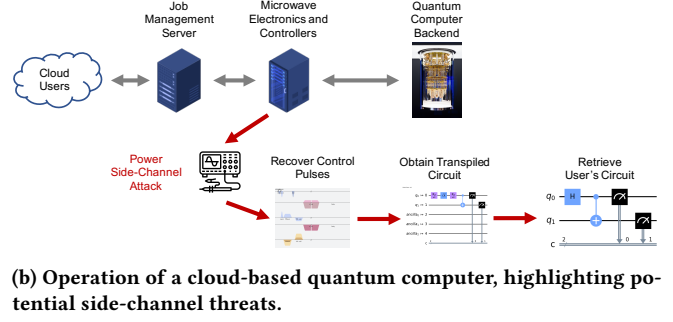
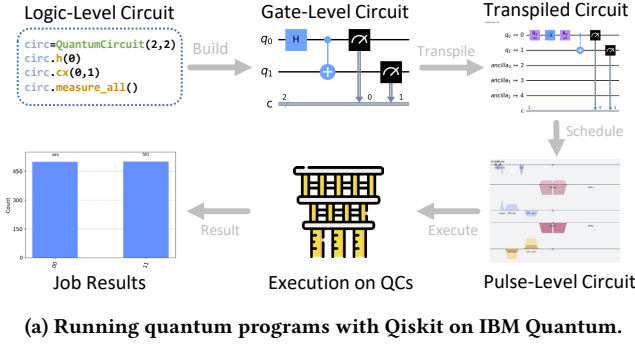


Figure 1: Process of running quantum circuits using Qiskit on IBM Quantum and the proposed threat model in the process.

## 2.2 Quantum Gates

Analogous to classical computing, the basic quantum operations at the logic-level are quantum gates. Quantum gates are unitary operations that modify the input qubits, and quantum algorithms consist of a series of quantum gates that can change input qubits into specific quantum states. A quantum gate  $U$  must satisfy the equation  $UU^\dagger = U^\dagger U = I$ , meaning that a quantum gate must be a unitary operation. A quantum gate  $U$  operating on a qubit  $|\psi\rangle$  can be written down as  $|\psi\rangle \rightarrow U|\psi\rangle$ . In the vector-matrix representation,  $2^n \times 2^n$  matrices can be used to express  $n$ -qubit quantum gates. For instance, the Pauli- $X$  gate, a single-qubit gate that flips  $|0\rangle$  to  $|1\rangle$  and  $|1\rangle$  to  $|0\rangle$ , is comparable to the NOT gate in classical computation. One another important example is the CNOT gate, also known as the CX gate, which is a two-qubit gate that if the control qubit is in the state  $|1\rangle$ , a Pauli- $X$  gate will be applied to the target qubit, and otherwise nothing will happen. Their matrix representations together with some other matrices of quantum gates are shown below. One thing to note is that we follow IBM Qiskit's [42] qubit order, where the leftmost qubit is the most significant and the rightmost qubit is the least significant. In light of this, the CX gate may have a different matrix representation in other papers if different qubit order is followed.

$$I = \begin{bmatrix} 1 & 0 \\ 0 & 1 \end{bmatrix}, X = \begin{bmatrix} 0 & 1 \\ 1 & 0 \end{bmatrix}, CX = \begin{bmatrix} 1 & 0 & 0 & 0 \\ 0 & 0 & 0 & 1 \\ 0 & 0 & 1 & 0 \\ 0 & 1 & 0 & 0 \end{bmatrix}$$

$$RZ(\theta) = \begin{bmatrix} e^{-i\frac{\theta}{2}} & 0 \\ 0 & e^{i\frac{\theta}{2}} \end{bmatrix}, SX = \frac{1}{2} \begin{bmatrix} 1+i & 1-i \\ 1-i & 1+i \end{bmatrix}$$

It has been demonstrated that any unitary quantum gate can be approximated within a minor error using only a small number of quantum gates [15]. Therefore, currently available quantum computers usually have a few basis gates, and by grouping the basis gates, they can form other quantum gates. It is not necessary and not possible for them to support all quantum gates. These basis gates, also called native gates, are one of the important configurations of quantum processors. Depending on the low-level control, different manufacturers or even different versions of quantum processors may have different native gates, which is a trade-off between many

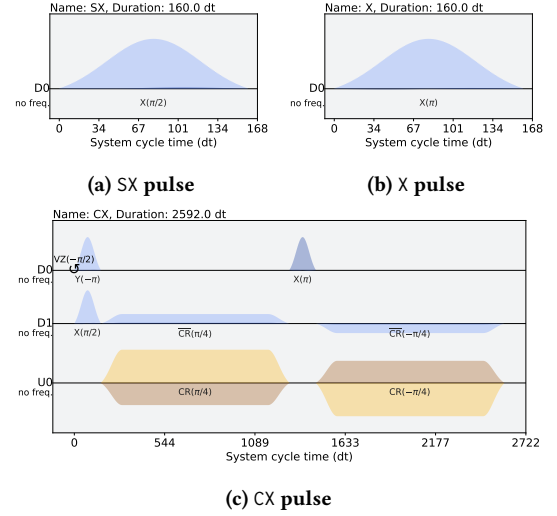


Figure 2: SX, X, and CX control pulses. All of the pulses are gathered on `ibm_lagos`. SX and X are on qubit 0, and CX is on qubit 0 and 1.

properties such as error rate and efficiency. In this paper, we based our experiments on IBM Quantum. As an example, for the majority of IBM Quantum quantum computers, the basis gates include I, RZ, SX, X, and CX. The matrix representations of these gates were shown above this paragraph. Before being run on the actual quantum computing hardware, other quantum gates, like the widely used Hadamard gate, must be decomposed into these basis gates.

## 2.3 Control Pulses

Superconducting qubits are usually controlled by microwave pulses. To actually perform each basis gate on a quantum computer, correct control pulses corresponding to each of the gates need to be generated and sent to the quantum computer. Examples of control pulses for SX, X, and CX gates are shown in Figure 2. On IBM Quantum, I gate does nothing and it only adds delays in the control pulses. RZ gate is a virtual gate and does not have any real pulse. More details about the virtual RZ gate will be discussed in Section 6.1.

A pulse is usually defined by the envelope, frequency, and phase. As an instance for the superconducting qubit control, the envelope specifies the shape of the signal which is generated by the arbitrary waveform generator (AWG), a common lab instrument, and the frequency and phase specify a period signal that will be used to modulate the envelope signal. These two signals together form the output signal that will be sent to the qubit. The typical settings to drive the qubits are shown in Figure 3.

To store envelopes, they are usually discretized into a series of time steps and each element specifies the amplitude at a specific time step. Though envelopes can be in any arbitrary pattern, they are usually parametrized by some predefined shapes so that only a few parameters are needed to specify the envelope. These parameters typically include the duration indicating the length of the pulse, the amplitude indicating the relative strength of the pulse, and other parameters specifying the shape of the pulse. For example, the Derivative Removal by Adiabatic Gate (DRAG) pulse [22, 38] is a standard Gaussian pulse with an additional Gaussian derivative component and lifting applied, and it can be specified with sigma that defines how wide or narrow the Gaussian peak is, and beta that defines the correction amplitude, as well as the duration and amplitude. Another example is the Gaussian square pulse which is a square pulse with a Gaussian-shaped risefall on both sides lifted such that its first sample is zero. Apart from the duration and amplitude, it is parametrized by sigma which defines how wide or narrow the Gaussian risefall is, the width that defines the duration of the embedded square pulse, and the ratio of each risefall duration to sigma.

On IBM Quantum, the pulses for all native gates are predefined while their parameters are frequently updated by calibrations so that they can maintain high fidelity over time. Pulse parameters are automatically measured and calibrated, and are ready to be used to generate the control pulses for quantum circuits.

## 2.4 Pulse-Level Circuit Description

To fully describe a quantum program, all pulses that need to be performed, when pulses should start relative to the starting point of the circuits, and to what qubits the pulses will be applied, need to be specified. This information together with other useful information forms a so-called *pulse-level circuit*.

Similar to how pulses are discretized, circuits are also discretized in time steps at the low-level. In this way, pulses can be conveniently fit into the circuits. In addition, it is also necessary to specify to which qubits quantum gates, measurements, and other operations should be applied. With all this information at hand, circuits can be well-defined and ready to be executed in quantum devices. After quantum circuits start to run, when the specified starting time steps are reached, the superconducting quantum computer control equipment sends the pulses defined by their information along electric lines to control the specified qubits.

## 2.5 Running Quantum Programs on Quantum Computers

To start the process of running a quantum program on nowadays cloud-based superconducting quantum computers, the quantum circuits that solve the desired problem need to be created first. Then

the quantum circuits go through a series of transforming processes, and are sent to the cloud to execute and finally users can get the results. We show a typical process of running quantum programs with Qiskit on IBM Quantum in Figure 1a.

The first step is to build the logic-level circuit with a quantum development kit, such as Qiskit [42], Braket SDK [4], Q# [36], Cirq [16].

The logic-level circuit can also be represented graphically, as shown in the “Gate-Level Circuit” in Figure 1a, lines that go from left to right stand in for qubits, while the symbols on the lines stand for operations. Without further information, qubits are typically thought to be in the  $|0\rangle$  state at the start of the quantum circuit. Qubits then evolve through left-to-right sequential processes and are controlled by quantum or classical operations denoted in the circuit plot. For the most part, measurements are performed at the end of the quantum circuit to measure, obtain, and store qubit data in classical memory for future evaluations.

Analogous to classical computing, quantum circuits are usually high-level instructions. Before executing the quantum circuits on quantum computers in reality, a series of operations need to be done to transform them into low-level and hardware-specific instructions, which is similar to the preprocessing, compilation, and assembly process for classical computing programs. To be specific, quantum circuits can be described using a number of different input methods and gates, but eventually, need to be converted to only the native gates supported by the quantum computer.

*Transpile* is the term used by Qiskit to stand for the operations and transformations that are like preprocessing and compilation. The process of transpiling involves many steps, including decomposing non-native quantum gates into groups of native gates, grouping and removing quantum gates to reduce the number of gates, mapping the logic qubits in the original circuits to the physical qubits on the specified quantum computers, routing the circuit under limited topologies, potentially optimizing circuits to lower error, and so on. After transpilation, circuits are modified based on hardware-specific knowledge and will generate the same logical results as the original circuits. Circuits up to this point are all gate-level circuits, which use a more general description so that they are understandable by people and can be portable in many cases, though they may still need to be transpiled if they are going to be performed on other kinds of quantum computers.

A lower-level step after transpilation is termed *schedule* in Qiskit. Scheduling further maps quantum circuits to microwave pulses, which are the ultimate physical operations used to regulate and control qubits. Because of this, scheduling transforms gate-level circuits into pulse-level circuits. Each microwave pulse is characterized by a series of parameters, such as amplitude and frequency, etc., discussed previously in Section 2.3. Based on previously calibrated data for each basis gate on each qubit or qubit pair and quantum gadget, scheduling creates microwave pulse sequences. Wave envelopes, frequencies, amplitudes, durations, and other parameters that characterize microwave pulses are included in the data. The final data contains all information that needs to be known by quantum computers to execute the program. After the quantum program starts, the equipment of quantum computers will be manipulated by this information, and qubits are controlled by the equipment to carry out quantum programs.

The steps discussed above convert the initial quantum circuits to a set of instructions that can be used to accomplish the specified quantum programs. As an example of running quantum programs, IBM Quantum provides Qiskit for users as the tool to design circuits, perform these steps, and submit quantum programs to the cloud, and finally, the cloud will execute the users' programs and return the results to users. The above-discussed process needs to be observed in general. In this process, scheduling and even transpilation can be omitted on the user side to simplify the overall development cycles, but they still need to be done on the server side.

## 2.6 Execution of Circuits and Shots

In nowadays quantum computing cloud platforms, quantum programs are usually submitted and executed in a particular pattern according to the platform settings. Because the results of most of the quantum algorithms are probabilistic, the same quantum algorithms usually need to be run many times to get the probabilistic results. One execution of the circuit is also often called one shot.

On IBM Quantum, users can submit one circuit or a list of circuits, and specifies how many shots the quantum jobs should run. When the quantum job starts, the quantum circuits are executed one by one sequentially. Between the quantum circuits, there is some reset mechanism to let qubits return to  $|0\rangle$  states, such as a long duration for qubits to decohere.

## 3 TREAT MODEL

### 3.1 Threat Model Background

**3.1.1 Channel.** As introduced in Section 2.3, pulses are applied to drive designated qubits. Which qubits should be controlled are specified by *channels*. It normally needs one channel for single-qubit gates and several channels for multiple-qubit gates. Channels can be mainly categorized into 4 types: drive channels that transmit signals to qubits that enact gate operations, control channels that provide supplementary control over the qubit to the drive channel, measure channels that transmit measurement stimulus pulses for readout, and acquire channels that are used to collect data. Drive channels and control channels are of more interest in this paper because they specify quantum gates. Generally speaking, drive channels correspond to qubits, and control channels correspond to connections between qubits. The number of channels of a quantum device is determined by its architecture. More specifically, the number of drive channels is usually equal to the number of qubits, and the number of control channels is usually equal to the number of connections between two qubits.

**3.1.2 Basis Pulse.** In Section 2.5, the typical process of running a quantum circuit is introduced. Every quantum circuit needs to be transpiled to a quantum circuit that contains only the basis gates of the target quantum device. We refer to the set of pulses after a basis gate is scheduled as its *basis pulses*. Because pulse parameters are highly dependent on qubit physical properties, while the quantum gate is an abstract concept, the same type of gate on different channels has different pulse parameters. For example,  $X$  gate on qubit 0 commonly has different pulse parameters from  $X$  gate on qubits other than 0. However, because basis gates and their pulse sets are predefined, they usually are the same.

**3.1.3 Basis Pulse Library.** The set of basis pulses of all basis gates is needed for scheduling. We refer to the set of pulses that defines all basis gates as *basis pulse library*. The information on basis pulses is provided by IBM Quantum for all their quantum devices. Notice that IBM Quantum also supports the so-called *custom pulse gates*, which allows users to perform gates calibrated with arbitrary pulses [43], and these gates are not changed in the transpilation and scheduling process. However, more work and a deeper understanding are needed for the correct utilization of this feature, and for most use cases, custom pulse gates are not needed. Therefore, in our assumption, we assume that the victim circuits do not contain any custom pulse gates.

**3.1.4 Power Trace.** Because pulses are needed to control superconducting qubits, these operations consume energy. We denote *power trace* as the time series of the power cost by the operations controlling qubits. The *total power trace* means the time series of the summation of the powers over all channels in a time period, while the *individual power trace* means the power trace on one specific channel. Suppose that there is equipment that can measure power consumption on some or all of the channels, and this measured power trace will consist of and depend on a number of channels.

## 3.2 Assumptions of Attacker Measurement

Our work assumes that an attacker has the ability to measure timing or power associated with the execution of quantum circuits. Specifically, we assume the attacker can measure these properties for each shot of a circuit, or they can measure a number of shots and it is easy to divide this into individual shots as discussed below, since all shots perform the same operations. Recall in Section 2.6, that each quantum program, i.e., quantum circuit, is executed multiple times, and each execution is called a *shot*. We assume physical access is common when considering power side-channel attacks in classical computers. Given the assumed physical access, timing information can also be obtained as discussed below.

**3.2.1 Per-Shot Timing Measurements.** We assume the attacker is able to measure the execution timing of the victim circuit. As shown in Figure 3, we assume the attacker is able to capture the traces of the control pulses. From the traces, the attacker can observe when pulses are occurring. In particular, the shots of a circuit are separated by inter-shot delay, which is used to reset the state of the qubits to  $|0\rangle$  before the next shot of a circuit is executed. Today this delay in superconducting qubit machines is on the order of 250 us, but will become longer as the decoherence times of the machines increase. The clear separation and the same pattern of the shots allow the attacker to measure their duration, and when one shot ends and the next begins.

**3.2.2 Per-Shot Power Measurements.** We assume the attacker is able to measure average power, and total energy, and collect power traces. As shown in Figure 4, we assume the attacker has access to the qubit drive equipment. From the arbitrary waveform generators or the mixer, we assume the attacker can collect the power data.

**3.2.3 Per-Channel Power Measurement.** As shown schematically in Figure 4 (A), we assume the attacker is able to collect per-channel

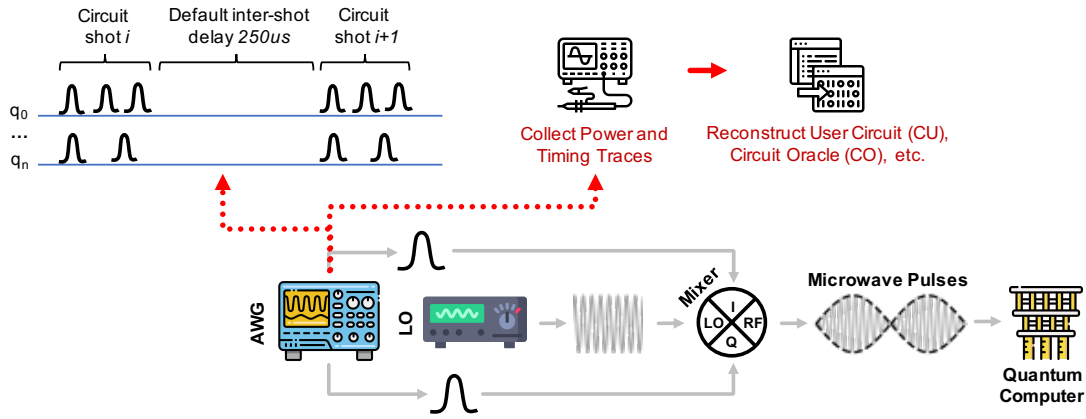


Figure 3: Schematic of a typical qubit drive setup. The local oscillator (LO) generates a low phase-noise microwave carrier signal, and then the wave is modulated in the IQ mixer by I and Q components generated by the arbitrary wave generator (AWG). The pulse is then sent to drive the qubits in the quantum computer. The red line shows the process to collect power traces, which can be exploited by attackers to retrieve information. The power traces also can reveal timing information by observing when the control pulses are occurring, as shown in the figure.

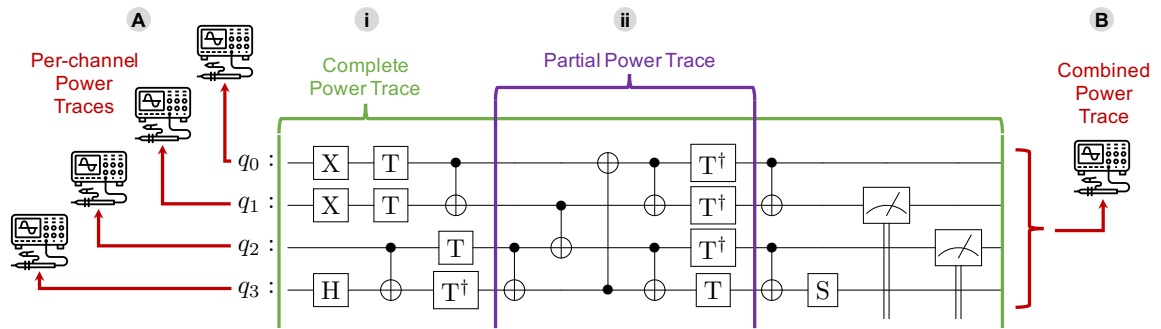


Figure 4: Quantum Computer power side-channel attack setups.

power traces; this corresponds to our Per-Channel Single Trace Attacks.

3.2.4 *Total Power Measurement.* A weaker attacker could be limited to collect only a single power trace of the combined channels, as shown in Figure 4 (B); this corresponds to our Total Power Single Trace Attacks.

3.2.5 *Single Power-Related Measurement.* Even weaker attackers may only get total energy or average power, which corresponds to our Single Measurement Attacks. Similarly, weak attackers may get only the timing of each shot, by observing the shot patterns with the inter-shot delays. This corresponds to our Timing Attack.

By collecting power traces for the duration of the shot, shown by Figure 4 (i), the attacker can deploy all of our proposed attacker’s goals in Sections 1.3. A more powerful attacker that has knowledge of the type of circuit running, but not the oracle or the ansatz used, or does not have the knowledge of the quantum processor on which the circuit ran, can measure power traces for specific portions of the shot, shown in Figure 4 (ii); this corresponds to our Circuit Oracle Identification (CO), Circuit Ansatz Identification (CA), and Quantum Processor Identification (QP) attacks.

### 3.3 Assumptions of Attacker’s Knowledge

We want to clarify that the attacker is assumed to know at all times: the information of quantum computers (number of qubits it contains, the topology and connections of the qubits) and the basis pulse libraries of them. We assume custom gates are not used by users, and all victim circuits are composed only of the basic gates supported by the quantum computer, typically including I, RZ, SX, X, and CX for IBM Quantum devices. Among the basic gates, we assume the RZ gates are virtual, as is common today. For an attacker who has only access to collect total power traces, we assume he or she knows the in-channel and cross-channel functions that define how the per-channel and total power traces correspond to the pulse information, which will be discussed in Section 4.2.

We assume the attacker knows when the victim circuits will be executed. Precise knowledge of the execution time is not needed as long as the attacker can capture the trace of one shot. Since the victim often executes thousands of shots, the attacker has multiple chances to capture at least one trace. Each shot is identical without considering the noise.

## 4 EXPERIMENT SETUP

### 4.1 Benchmarks Used

In this paper, we used QASMBench Benchmark Suite version 1.4 [30] for NISQ evaluation. Unless otherwise specified, `ibm_lagos`, a 7-qubit H-shape superconducting quantum computer (coupling map is shown in Figure 7c) is used for transpilation and scheduling. Due to the limitation of the number of qubits of `ibm_lagos`, we chose all algorithms whose numbers of qubits are less or equal to 7. Detailed information about the benchmark can be found in Table 1.

We removed benchmarks “`ipea`” (iterative phase estimation algorithm) and “`shor`” (Shor’s algorithm) for evaluation because they have Reset and middle measurement that cannot be scheduled on `ibm_lagos` due to lack of basis pulses. Without otherwise specified, we used `seed_transpiler = 0` to control the randomness and other default parameters for transpilation.

### 4.2 Power Traces

We refer *in-channel* and *across-channel functions* as the functions for computing the per-channel power traces and the total power traces from pulse information. The in-channel function, which we denote as  $Power_c[p_c(x)]$ , where  $c$  represents the channel and  $p_c(x)$  represents the pulse amplitude time series on that channel, specifies how the per-channel power traces are computed from pulse amplitude. The across-channel function, which we denote as  $Total[f_{c_1}(x), \dots, f_{c_n}(x)]$ , where  $c_i, i \in \{1, \dots, n\}$  represent all the channels of one quantum processor, specifies how the total power traces are summed up from all per-channel power traces  $f_c(x)$ . Based on these definitions, the total power traces  $P(x)$  can be computed from the per-channel pulse amplitude time series  $p_{c_i}(x)$ :

$$P(x) = Total \{Power_{c_1}[p_{c_1}(x)], \dots, Power_{c_n}[p_{c_n}(x)]\} \quad (1)$$

In the experiment, the total power traces, the per-channel power traces, and the pulse amplitude time series are all one-dimensional time series. To simulate the in-channel and across-channel functions, we assume:

$$Power_c[p_c(x)] = \text{Re}^2[p_c(x)] + \text{Im}^2[p_c(x)] \quad (2)$$

and:

$$Total[f_{c_1}(x), \dots, f_{c_n}(x)] = \sum_{i \in \{1, \dots, n\}} f_{c_i}(x) \quad (3)$$

which means the per-channel power traces are the square of the norm of the amplitude, and the total power traces are directly the summation of per-channel power traces with the same weight.

In our experiments, we obtained the pulse information from Qiskit APIs provided by IBM Quantum on each of the target quantum computers. From the pulse information, we computed the per-channel and the total power traces using the above functions.

### 4.3 Circuit Norm and Distance

To evaluate the results, we define 3 metrics: *circuit norm*, *circuit distance* between two circuits, and *normalized circuit distance* between two circuits, all of which are in terms of the total power traces:

- (1)  $norm(C)$ : the circuit norm of the circuit  $C$  with the total power traces  $P_C(x)$  is  $f_{norm}[P_C(x)]$
- (2)  $dist(C_1, C_2)$ : the circuit distance of the circuit  $C_1$  and the circuit  $C_2$  is  $f_{dist}[P_{C_1}(x), P_{C_2}(x)]$ .

- (3)  $norm\_dist(C_1, C_2)$ : the normalized circuit distance of the circuit  $C_1$  and the circuit  $C_2$  is  $\frac{1}{norm(C_1)} dist(C_1, C_2)$ .

The definitions depend on the choice of the norm  $f_{norm}$  and distance function  $f_{dist}$ . In this paper, we choose the Euclidean norm and distance for these two functions, i.e.,  $f_{norm}(\vec{a}) = \sqrt{\sum_{i=1}^n a_i^2}$  and  $f_{dist}(\vec{a}, \vec{b}) = \sqrt{\sum_{i=1}^n (a_i - b_i)^2}$ .

## 5 EVALUATION

### 5.1 User Circuit Identification (UC)

To further expand the circuit list, we chose different initial layouts in the transpilation so that the same circuit can be transpiled into different circuits based on the hardware configuration. For an  $n$ -qubit circuit on  $k$ -qubit backend, the number of initial layouts is in total  $\binom{n}{k}$ . In the experiment, we chose 8 circuit lists  $CL_i$ , where  $i$  is the number of initial layouts. We choose  $i$  to be 1, 2, 4, 8, 16, 32, 64, 128. The exact initial layout is randomly selected from  $\binom{n}{7}$  initial layouts. If for one circuit,  $i > \binom{n}{7}$ , which means there are not enough initial layouts, then we choose all the  $\binom{n}{7}$  permutations as the initial layouts. For reference, after expanding, the number of circuits in the circuit list is listed in Table 2.

Besides the total power traces, three additional physical quantities are also used to evaluate the results: energy, mean power, and duration of the circuit. The energy is simulated by adding all terms of the one-dimensional total power time series, which is the total energy in the dt unit of the circuit. The duration is the time from the start to the end of the circuit in the dt unit, which is also the same as the length of the one-dimensional total power time series. The mean power is then computed by dividing the energy by the duration. For a circuit  $C$ , we used  $v_p(C)$ ,  $v_e(C)$ ,  $v_m(C)$ , and  $v_d(C)$  to represent these values.

For the experiment of identifying user circuits from the knowledge of possible circuits, we define the accuracy under some experiment settings to be the proportion of circuits in the circuit list that are correctly identified. More specifically, for each circuit  $C \in CL_i$ , we calculated the distance  $dist(x)$  (see Section 4.3) with the physical quantity  $q(x)$  between it and all the circuits in the list:

$$dist[q(C), q(C')], \forall C' \in CL_i \quad (4)$$

The identification for the circuit  $C$  is chosen to be the circuit with the smallest distance between the measured and the software-generated physical quantities of this circuit:

$$id_{i,q}(C) = \min_{C' \in CL_i} dist[q(C), q(C')] \quad (5)$$

In the case of UC, it is assumed that the attacker knows a list of quantum circuits, and the victim circuit is chosen from this list. The attacker has access to all circuits in the list, and the attacker measured the power traces of victim circuits. The goal of the attacker is to find the correct circuits from which the power traces were generated.

Figure 5a – Figure 5c shows the energy, mean power, and duration of the original benchmark. The distribution gives an insight into how these physical quantities perform in identifying user circuits. Based on the experiment setup above, we computed the accuracy, which is shown in Figure 6. As the figure shows, though power-related traces are harder to gather than timing traces, they

| Benchmark         | Description                                    | Algorithm             | Reference |
|-------------------|--|-----------------------|-----------|
| deutsch           | Deutsch algorithm with 2 qubits for $f(x) = x$ | Hidden Subgroup       | [13]      |
| iswap             | An entangling swapping gate                    | Logical Operation     | [13]      |
| quantumwalks      | Quantum walks on graphs with up to 4 nodes     | Quantum Walk          | [33]      |
| grover            | Grover’s algorithm                             | Search/Optimization   | [2]       |
| ipea*             | Iterative phase estimation algorithm           | Hidden Subgroup       | [13]      |
| dnn               | 3 layer quantum neural network sample          | Machine Learning      | [45]      |
| teleportation     | Quantum teleportation                          | Quantum Communication | [21]      |
| qaoa              | Quantum approximate optimization algorithm     | Search/Optimization   | [27]      |
| toffoli           | Toffoli gate                                   | Logical Operation     | [28]      |
| linearsolver      | Solver for a linear equation of one qubit      | Linear Equation       | [12]      |
| fredkin           | Controlled-swap gate                           | Logical Operation     | [28]      |
| wstate            | W-state preparation and assessment             | Logical Operation     | [13]      |
| basis_change      | Transform the single-particle basis            | Quantum Simulation    | [31]      |
| qrng              | Quantum random number generator                | Quantum Arithmetic    | [47]      |
| cat_state         | Coherent superposition of two coherent states  | Logical Operation     | [28]      |
| inverseqft        | exact inversion of quantum Fourier transform   | Hidden Subgroup       | [13]      |
| adder             | Quantum ripple-carry adder                     | Quantum Arithmetic    | [28]      |
| hs4               | Hidden subgroup problem                        | Hidden Subgroup       | [28]      |
| bell              | Circuit equivalent to Bell inequality test     | Logic Operation       | [17]      |
| qft               | Quantum Fourier transform                      | Hidden Subgroup       | [13]      |
| variational       | Variational ansatz for a Jellium Hamiltonian   | Quantum Simulation    | [31]      |
| vqe_uccsd         | Variational quantum eigensolver with UCCSD     | Linear Equation       | [28]      |
| basis_trotter     | Trotter steps for molecule LiH at equilibrium  | Quantum Simulation    | [31]      |
| qec_sm            | Repetition code syndrome measurement           | Error Correction      | [13]      |
| lpn               | Learning parity with noise                     | Machine Learning      | [44]      |
| qec_en            | Quantum repetition code encoder                | Error Correction      | [44]      |
| shor*             | Shor’s algorithm                               | Hidden Subgroup       | [24]      |
| pea               | Phase estimation algorithm                     | Hidden Subgroup       | [13]      |
| error_correction3 | Error correction with distance 3 and 5 qubits  | Error Correction      | [34]      |
| simons            | Simon’s algorithm                              | Hidden Subgroup       | [2]       |
| qaoa              | Quantum approximate optimization algorithm     | Search & Optimization | [17]      |
| vqe_uccsd         | Variational quantum eigensolver with UCCSD     | Linear Equation       | [28]      |
| hhl               | HHL algorithm to solve linear equations        | Linear Equation       | [25]      |

\* These circuits contain the middle measurement and Reset gate, and cannot be scheduled on the backend currently because their basis pulses are not provided.

**Table 1: QASMBench Benchmark Suite version 1.4 [30].**

| No. Layouts  | 1  | 2  | 4   | 8   | 16  | 32  | 64   | 128  |
|--------------|----|----|-----|-----|-----|-----|------|------|
| No. Circuits | 31 | 62 | 124 | 248 | 496 | 992 | 1874 | 3538 |

**Table 2: Number of circuits in the circuit list with different numbers of layouts.**

have a better performance when identifying user circuits. As the number of layouts increases, the accuracy computing by duration decreases much more than power-related metrics. One reason is that duration is in dt unit, making it easier to be the same for different circuits, while power-related metrics are more distinct from each other. In addition to the distinguishability, it is easier to protect from timing attacks by adding delay gates to change the duration to make the duration of quantum circuits in the list to be

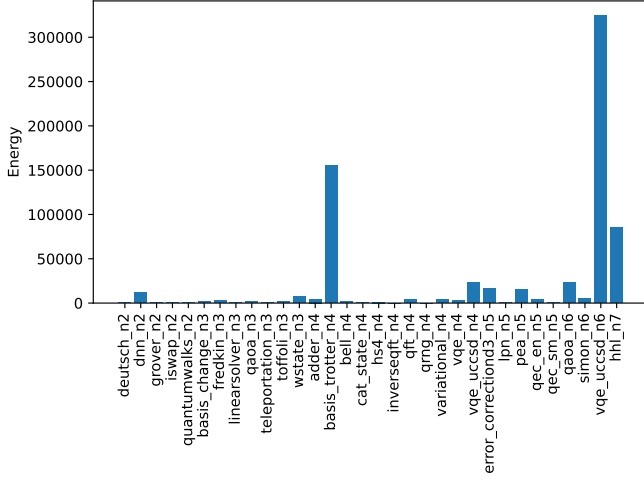
the same, but it is harder to hide the information about the power or energy without changing the function of the quantum circuits.

## 5.2 Circuit Oracle Identification (CO)

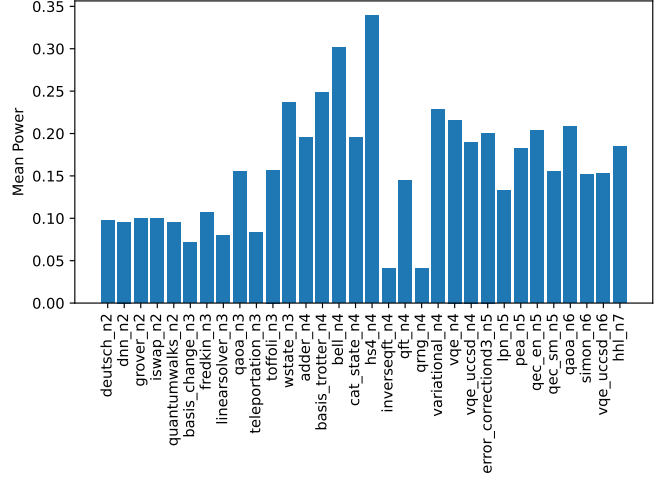
Many quantum algorithms consist of oracles, which act like black boxes that return desired quantum states based on the input. For example, a *Boolean oracle* change the input states to another binary representation, i.e.,  $U_f |x\rangle \otimes |0\rangle = |x\rangle \otimes |f(x)\rangle$ ; a *phase oracle* does not change the state but change its phase, i.e.,  $P_f |x\rangle = (-1)^{f(x)} |x\rangle$ .

For CO, we choose three textbook algorithms for how the oracle can be identified with the quantum computing power side-channels:

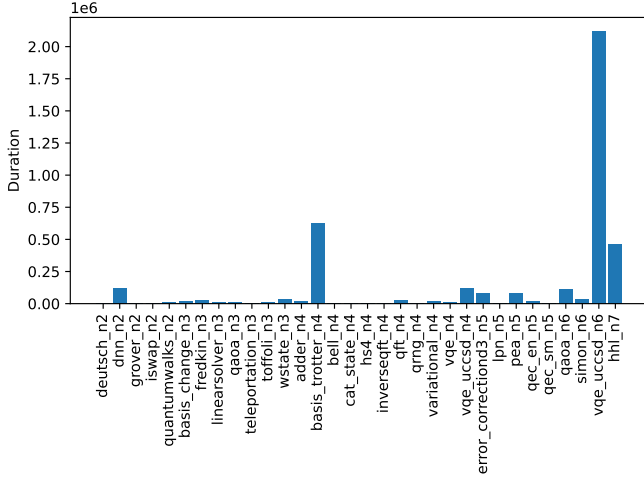
- (1) Bernstein-Vazirani (BV) [9]: given an oracle  $f(x) = s \cdot x$ , find the hidden  $s$  in the oracle.
- (2) Deutsch-Jozsa (DJ) [14]: given an oracle  $f(x) = 0$  or  $1$ , which is either a constant function whose outputs are all 0 or all 1,



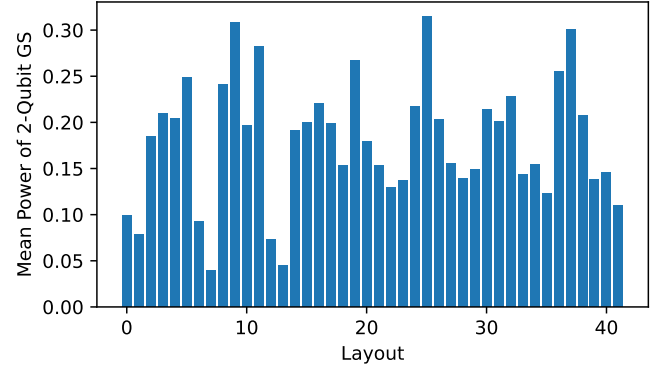
(a) Energy of the benchmark.



(b) Mean power of the benchmark.



(c) Duration of the benchmark.



(d) Mean power of 2-qubit Grover's search with different initial layouts.

Figure 5: Energy, mean power, and duration of the circuits in the benchmark.

or a balanced function whose outputs are half 0 and half 1, find whether the oracle is constant or balanced.

- (3) Grover's Search (GS) [23]: given an oracle  $f(x)$  to reflect the states, find a state specified by the oracle.

All these algorithms can have an arbitrary number of qubits. We tested from 1-qubit to 6-qubit versions, and for all the  $n$ -qubit algorithms, the parameters specifying the oracles are tested from  $0 \dots 0$  to  $1 \dots 1$ . Since if the function for DJ is constant, the oracle can be an empty circuit, we only tested the balanced function.

The minimum normalized circuit distance is used to evaluate the results, shown in Table 3. For BV, since the oracles are quite different from each other, the minimum circuit distance is not 0, which means the oracles can be distinguished from each other. However, for DJ and GS, the circuits for different oracles can be the same, and the only changes are the angles of the rotation gates, such

| Algorithm          | Number of Qubits/Oracles |      |      |      |      |      |
|--------------------|--------------------------|------|------|------|------|------|
|                    | 1/2                      | 2/4  | 3/8  | 4/16 | 5/32 | 6/64 |
| Bernstein-Vazirani | 1.00                     | 0.30 | 0.07 | 0.06 | 0.07 | 0.06 |
| Deutsch-Jozsa      | 0.00                     | 0.00 | 0.00 | 0.00 | 0.00 | 0.00 |
| Grover's Search    | 0.00                     | 0.00 | 0.00 | 0.00 | 0.00 | 0.00 |

Table 3: Evaluation for circuit oracle identification (CO). Normalized circuit distance for Bernstein-Vazirani, Deutsch-Jozsa, and Grover's Search with the number of qubits from 1 to 6 on ibm\_lagos. Bernstein-Vazirani and Deutsch-Jozsa need one additional qubit to control the oracle.

as RZ gate. Since RZ is a virtual gate on IBM quantum backends with no duration and amplitudes, all circuits have the same power traces

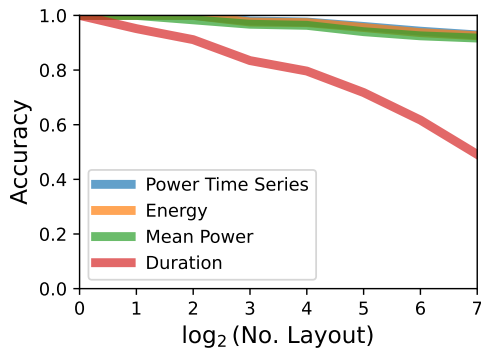


**Figure 6: Evaluation for user circuit identification (UC). Accuracy based on 4 metrics: power time series, energy, mean power, and duration. The circuit list is expanded by transpiling the benchmark with a number of initial layouts.**

and thus cannot be distinguished from each other. More details of the virtual RZ gate will be discussed in Section 6.1.

Another thing that needs to pay attention for circuit oracle identification is that circuits after transpilation are highly dependent on the transpiler settings. For example, the oracles of some algorithms have symmetries, such as 3-qubit Bernstein-Vazirani with "01" and "10" as the hidden string, the transpiler may output the same circuits. This can be achieved by changing the bit order of the measurement results. In our experiment, to show that quantum computer power side-channels can be exploited to retrieve the information of oracles, we forced the initial layouts of all circuits to be the same to avoid such transpilation.

### 5.3 Circuit Ansatz Identification (CA)

One important application of quantum computing is solving optimization problems, such as finding the minimum eigenvalue of a matrix. The Variational Quantum Eigensolver (VQE) [40] and the Quantum Approximate Optimization Algorithm (QAOA) [20] are the representative quantum algorithms for optimization. Besides, quantum machine learning [10] and quantum deep learning [51] are also actively researched. These algorithms solve the optimization problem by generating appropriate quantum states through parameterized circuits and iteratively updating parameters to find the extremes. These circuits are also often called *ansatz*.

For identifying circuit ansatz, we chose 6 ansatz circuits from the benchmark, "qaoa\_n3", "variational\_n4", "vqe\_n4", "vqe\_uccsd\_n4", "qaoa\_n6", "vqe\_uccsd\_n6", and computed the minimum normalized circuit distance between these circuits, which is 0.970. Such a large normalized circuit distance proves the ability to effectively distinguish them.

In addition to the ansatz circuit configuration, another important piece of information about the ansatz circuit is its parameters. However, due to the same reason discussed in Section 5.2 why oracle for Deutsch-Jozsa or Grover's search cannot be identified, the parameters usually only change the rotational angles of the virtual RZ gates in the ansatz circuit, while other real gates remain the same, it is impossible to retrieve any information from the power

traces about the parameters. More discussion about the virtual RZ gate will be discussed in Section 6.1.

### 5.4 Qubit Mapping Identification (QM)

As discussed in previous sections, the pulses for one quantum gate on different qubit or qubit pairs are different since the pulses need to be calibrated based on the qubit's physical properties to achieve the same logical operations. Thus, the power traces also encode the information of the quantum processor on which the circuit was executed. This information includes the physical qubits to which the quantum gates are applied, and this motivates the goal of identifying the qubit mapping of the quantum circuit. For example, Figure 5d shows the mean power of 2-qubit Grover's search with different initial layouts.

Before the quantum circuit is executed on the quantum device, the mapping from the logical qubits to the physical qubits must be specified. In the transpilation process of Qiskit, the qubit mapping is automatically selected if no input for the layout is given. In the experiment, we selected 10 initial layouts for each circuit in the benchmark, and compute the minimum normalized circuit distance in the circuit list.

The results are shown in the QM column of Table 4. Nearly all the benchmark has a large minimum normalized circuit distance, which indicates that they can be well distinguished from each other. However, the minimum normalized circuit distance of "inverseqft" (inverse quantum Fourier transformation) and "qrng" (quantum random number generator) is 0. The reason is that the circuits for both these algorithms only consist of single-qubit gates ("inverseqft" also has the dynamical RZ gate), so when changing the order of the qubits in the initial layout, it does nothing to the circuit. For example, the circuits with initial layout [0, 1, 2, 3] and [1, 0, 2, 3] are the same, and therefore the circuit distance is 0 between these two circuits with such initial layouts. However, the circuit distance is not 0 if the initial layouts contain at least 1 different qubit.

### 5.5 Quantum Processor Identification (QP)

Another kind of hardware-related information can be the quantum processor on which the circuit was executed. Not only the basis pulse library, but also the coupling map plays a role in determining the power traces. The identification among quantum processors with distinct connections may be easier for circuits with a large number of qubits since it needs to add switch gates to the circuit and the information of quantum processors is encoded in terms of connections. Nevertheless, the identification among quantum processors with the same coupling map is also feasible since the properties of qubits are distinct across quantum processors and this information is included in the basis pulse library.

We selected 9 IBM-Q quantum devices to show the diversity among quantum devices: ibmq\_lima, ibmq\_quito, ibmq\_belem, ibmq\_manila, ibmq\_jakarta, ibmq\_oslo, ibmq\_nairobi, ibmq\_lagos, ibmq\_perth. The former 4 devices are 5-qubit and the others are 7-qubit devices. There are two coupling maps for 5-qubit devices: line-shape shown in Figure 7a and T-shape shown in Figure 7b, and only one coupling map for the 7-qubit devices: H-shape shown in Figure 7c. The statistics of the amplitude of X and SX gates on different qubits are shown in Figure 7d and Figure 7e, and the statistics

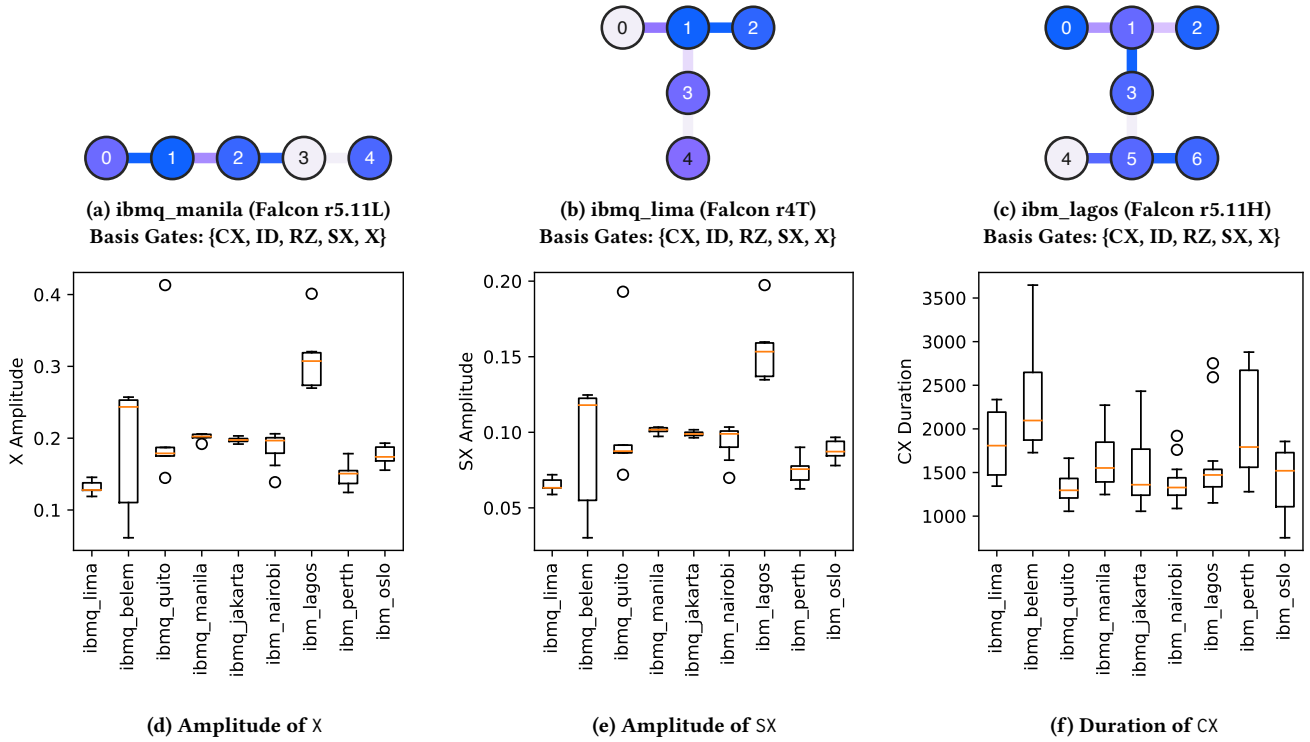


**Figure 7: IBM-Q device information.** (a) – (c) Three coupling maps of the IBM-Q devices. The color of nodes implies the frequency (GHz) of the qubit. The connection color implies the gate time in nanoseconds for 2-qubit gates such as CX. (d) – (e) Box plots of amplitude of X and SX and duration of CX on 9 IBM Quantum backends.

of the duration of CX gates is shown in Figure 7f. All of them have distinct features in the basis pulse library. Note that the distribution of X and SX are the same. This is due to that only X is calibrated, and the amplitude of SX is directly set to be half of the amplitude of X. The disparity in amplitude and duration makes it viable to identify and reconstruct the circuits from their power traces.

To quantify the influence of the difference of the connectivity and basis pulse library over backends on the total power traces of quantum circuits, we transpiled the benchmark on these 9 quantum devices. The QP column of Table 4 shows the minimum normalized circuit distance over these devices. Most of the circuits have large enough circuit distances over different quantum devices, making them straightforward to be separated individually. In addition, “inverseqft” and “qrng” may not be determined for qubit mapping identification, but they are possible to be recognized for quantum processor identification.

### 5.6 Reconstruction from Power Traces (RP)

If the attacker has the access to the basis pulse library, they can readily reconstruct the circuit from the gathered per-channel power traces. We implement the algorithm to reconstruct the circuit and the results are shown in the RP column of Table 4. We can successfully reconstruct all circuits in the benchmark given their per-channel power traces.

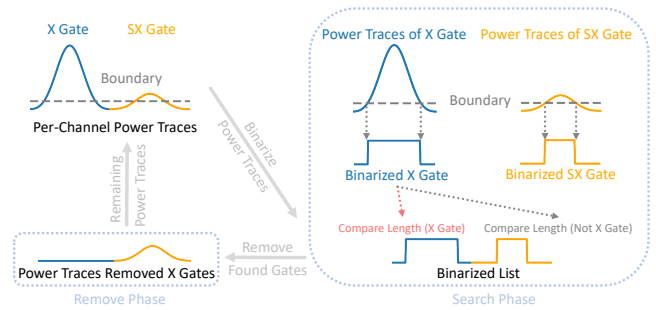


**Figure 8: Algorithm for reconstructing circuits from power traces.** The algorithm includes two phases: the search phase and the remove phase. In the search phase, the algorithm binarizes the power traces and searches for a target gate in the power traces by comparing the length of the binary segments with the length of the binarized power traces of the basis gates. In the remove phase, the algorithm removes all the target gates from the power traces and generates the new power traces for the next iteration.

The algorithm is shown in Figure 8. The algorithm iterates all channels and finds the corresponding pulses. The algorithm includes two phases: the *search phase* and *remove phase*. In the search phase, the algorithm locates all gates in the power traces and selects

| Benchmark     | Qubits | Gates | CXs  | QM    | QP    | RP |
|---------------|--------|-------|------|-------|-------|----|
| deutsch       | 2      | 10    | 1    | 0.025 | 0.116 | ✓  |
| dnn           | 2      | 306   | 42   | 0.039 | 0.116 | ✓  |
| grover        | 2      | 15    | 2    | 0.143 | 0.116 | ✓  |
| iswap         | 2      | 14    | 2    | 0.143 | 0.116 | ✓  |
| quantumwalks  | 2      | 38    | 3    | 0.125 | 0.117 | ✓  |
| basis_change  | 3      | 85    | 10   | 0.673 | 0.068 | ✓  |
| fredkin       | 3      | 31    | 17   | 0.800 | 0.411 | ✓  |
| linearsolver  | 3      | 26    | 4    | 0.735 | 0.080 | ✓  |
| qaoa          | 3      | 35    | 9    | 0.546 | 0.570 | ✓  |
| teleportation | 3      | 12    | 2    | 0.473 | 0.075 | ✓  |
| toffoli       | 3      | 24    | 9    | 0.096 | 0.573 | ✓  |
| wstate        | 3      | 47    | 21   | 0.789 | 0.101 | ✓  |
| adder         | 4      | 33    | 16   | 0.727 | 0.201 | ✓  |
| basis_trotter | 4      | 2353  | 582  | 0.895 | 0.220 | ✓  |
| bell          | 4      | 53    | 7    | 0.781 | 0.196 | ✓  |
| cat_state     | 4      | 6     | 3    | 0.744 | 0.241 | ✓  |
| hs4           | 4      | 28    | 4    | 0.545 | 0.327 | ✓  |
| inverseqft    | 4      | 30    | 0    | 0.000 | 0.001 | ✓  |
| qft           | 4      | 50    | 18   | 0.817 | 0.287 | ✓  |
| qrng          | 4      | 12    | 0    | 0.000 | 0.001 | ✓  |
| variational   | 4      | 58    | 16   | 0.792 | 0.239 | ✓  |
| vqe           | 4      | 73    | 9    | 0.660 | 0.194 | ✓  |
| vqe_uccsd     | 4      | 238   | 88   | 0.858 | 0.241 | ✓  |
| error_c3      | 5      | 249   | 61   | 0.855 | 0.220 | ✓  |
| lpn           | 5      | 17    | 2    | 0.576 | 0.194 | ✓  |
| pea           | 5      | 126   | 57   | 0.874 | 0.210 | ✓  |
| qec_en        | 5      | 52    | 16   | 0.746 | 0.250 | ✓  |
| qec_sm        | 5      | 8     | 4    | 0.573 | 0.266 | ✓  |
| qaoa          | 6      | 408   | 84   | 0.869 | 0.283 | ✓  |
| simon         | 6      | 65    | 23   | 0.796 | 0.605 | ✓  |
| vqe_uccsd     | 6      | 2289  | 1199 | 0.906 | 0.278 | ✓  |
| hhl           | 7      | 1092  | 298  | 0.873 | 0.317 | ✓  |

**Table 4: Evaluation for qubit mapping (QM) identification, quantum processor (QP) identification, and reconstruction from power traces (RP). The numbers of gates are based on circuits transpiled on `ibm_lagos` with `seed_transpiler = 0` and other default arguments. The minimum normalized circuit distance is used to evaluate the results for QM and QP. For RP, the checkmark shows the original circuit is correctly reconstructed given the per-channel power traces.**

the target gate. In the remove phase, the algorithm removes all the target gates from the power traces and generates new power traces without the removed gates for the next iteration.

While multi-qubit gates may include several pulses on several channels, and some of these pulses may have the same shape as the single-qubit pulses, our implementation first iterates all control channels and find all multi-qubit gates. After locating all multi-qubit gates, the algorithm removes them from the per-channel power traces. Then a similar process is done for single-qubit gates. The algorithm iterates the remaining drive channels and locates specific

single qubit gates, and then removes them from the per-channel power traces. After iterating all channels and all basis gates, the found gates and their start times are the output of the algorithm.

For IBM-Q quantum devices, there are only three real gates,  $X$ ,  $SX$ , and  $CX$ . The pulse shapes of all these gates are Gaussian-related, such as the Derivative Removal by Adiabatic Gate (DRAG) pulse or Gaussian Square. Based on these characteristics, we transform the goal of finding the pulses in the power traces into finding the segment in the binary list. This is done by binarizing the per-channel traces based on an input boundary, i.e., if the power is larger than the boundary, its value is set to be 1, and set to 0 if not. The same process is also done for the software-generated power traces of basis gates. After binarizing, the per-channel power traces are transformed into a list of continuous 1s and 0s if the boundary is correctly set to be between 0 and the maximum of the amplitude. Then the pulses can be identified by classifying segments of 1s.

There are two ways to determine the gates. The first way is to use a uniform boundary, and because  $X$  and  $SX$  have the same duration but different amplitude, and the pulse shapes are similar to the Gaussian function and they do not have any abrupt change, their binary forms have different lengths. The type of gate can be identified by comparing the length of the segment in the binary list with the length of the binary form of the power traces of basis pulses. The second way is to use different boundaries in the search phase, i.e., firstly set a boundary between the maximum of the power traces of  $X$  and  $SX$ , so only  $X$  can be found. After removing  $X$ , then set a boundary between 0 and the maximum of the power traces of  $SX$ . The start time can be easily computed at the same time and set to the granularity of the quantum device, where the pulses must start at multiples of the granularity.

The binarizing process is to make the method more robust under measurement noise. Another parameter for robustness is tolerance, which means the allowed length difference when comparing the length of the segment in the binary list and the length of the binary form of the power traces of the basis gate. If the difference between these two is in the range of tolerance, then it is chosen to be identified. The boundary and the tolerance are coupled in the way that the binary form of the power of one basis gate cannot be mixed with another in the range of the tolerance.

## 6 DEFENSES

In this section, we present a possible defense against quantum computer power-side channel attacks.

### 6.1 Defense via Virtual RZ Gate Substitution

RZ gate is usually one of the basis gates in superconducting quantum computers, which rotates a single qubit around the Z axis in the Bloch sphere. While other basis gates have their calibrated pulses, RZ gate can be implemented easily as a virtual gate with the arbitrary wave generators (AWG) [29, 32]. If RZ gate is implemented as a virtual gate, then it will be "perfect", i.e., no actual pulses are needed and thus it takes no time to execute. As we assume that the power consumption depends on the amplitudes of pulses, RZ gate is undetectable in power-side channels on the quantum devices where it is designed to be virtual. Virtual RZ gate is valuable because any

arbitrary SU(2) gate can be decomposed as [32]:

$$U(\theta, \phi, \lambda) = Z_{\phi-\pi/2} X_{\pi/2} Z_{\pi-\theta} X_{\pi/2} Z_{\lambda-\pi/2} \quad (6)$$

where  $Z_{\theta}$  is RZ gate with the rotational angle  $\theta$  and  $X_{\pi/2}$  is RX gate with rotational angle  $\pi/2$ , or SX gate with a global phase. Therefore, any single-qubit gates can be realized with only  $X_{\pi/2}$  and virtual RZ gate.

To protect quantum computers from power-side channel attacks, RZ gate can be added to form a new circuit that is logically equivalent to the original circuits. With randomized compiling, it is proved that the new circuit can be generated while only introducing a little or no experimental overhead [48]. More formally, the virtual RZ gate scheme is to change one quantum gate  $U$  to  $A$  and  $B$ :

$$U = U_1 \cdots U_k \quad (7)$$

where at least one  $U_i, i \in 1, \dots, k$  is  $RZ(\theta)$  and  $U$  and  $U_{i_1} \cdots U_{i_n}$  are not equivalent. By modifying the circuit and replacing randomly selected gates with equivalent gate sequences that contain RZ gates, the attacker will not be able to reconstruct the original circuit fully from the power traces since he or she does not know where the RZ gates are, and what are the rotation angles.

## 7 CONCLUSION

This work presented the first exploration of power side-channels of quantum computers. We propose the threat model and several applications of quantum computer power side-channels, and evaluate how effective power traces can be used in the various cases. As this work shows, power side-channels attacks could be powerful and practical for inferring secret information about circuits executing on quantum computers.

## REFERENCES

- [1] Arnold Abromeit, Florian Bache, Leon A Becker, Marc Gourjon, Tim Güneysu, Sabrina Jörn, Amir Moradi, Maximilian Ortl, and Falk Schellenberg. 2021. Automated masking of software implementations on industrial microcontrollers. In *2021 Design, Automation & Test in Europe Conference & Exhibition (DATE)*. IEEE, 1006–1011.
- [2] AgentANAKIN. 2019. Grover’s Algorithm. <https://github.com/AgentANAKIN/Grover-s-Algorithm>.
- [3] Giovanni Agosta, Alessandro Barengi, and Gerardo Pelosi. 2019. Compiler-based techniques to secure cryptographic embedded software against side-channel attacks. *IEEE Transactions on Computer-Aided Design of Integrated Circuits and Systems* 39, 8 (2019), 1550–1554.
- [4] Amazon Braket SDK. 2023. <https://docs.aws.amazon.com/braket/latest/developer/guide/api-and-sdk-reference.html>.
- [5] Amazon Web Services. 2023. Amazon Braket. <https://aws.amazon.com/braket/>
- [6] Ali Galip Bayrak, Francesco Regazzoni, David Novo, Philip Brisk, François-Xavier Standaert, and Paolo Ienne. 2013. Automatic application of power analysis countermeasures. *IEEE Trans. Comput.* 64, 2 (2013), 329–341.
- [7] Sonia Belaïd, Pierre-Évariste Dagand, Darius Mercadier, Matthieu Rivain, and Raphaël Wintersdorff. 2020. Tornado: Automatic generation of probing-secure masked bitsliced implementations. In *Annual International Conference on the Theory and Applications of Cryptographic Techniques*. Springer, 311–341.
- [8] Nicolas Belleville, Damien Couroussé, Karine Heydemann, and Henri-Pierre Charles. 2018. Automated software protection for the masses against side-channel attacks. *ACM Transactions on Architecture and Code Optimization (TACO)* 15, 4 (2018), 1–27.
- [9] Ethan Bernstein and Umesh Vazirani. 1997. Quantum Complexity Theory. *SIAM J. Comput.* 26, 5 (1997), 1411–1473. <https://doi.org/10.1137/S0097539796300921>
- [10] Jacob Biamonte, Peter Wittek, Nicola Pancotti, Patrick Rebentrost, Nathan Wiebe, and Seth Lloyd. 2017. Quantum machine learning. *Nature* 549, 7671 (2017), 195–202.
- [11] Arthur Blot, Masaki Yamamoto, and Tachio Terauchi. 2017. Compositional synthesis of leakage resilient programs. In *International Conference on Principles of Security and Trust*. Springer, 277–297.
- [12] Cyril Branciard, Nicolas Gisin, Barbara Kraus, and Valerio Scarani. 2005. Security of two quantum cryptography protocols using the same four qubit states. *Physical Review A* 72, 3 (2005), 032301.
- [13] Andrew W Cross, Lev S Bishop, John A Smolin, and Jay M Gambetta. 2017. Open quantum assembly language. *arXiv preprint arXiv:1707.03429* (2017).
- [14] David Deutsch and Richard Jozsa. 1992. Rapid solution of problems by quantum computation. *Proceedings of the Royal Society of London. Series A: Mathematical and Physical Sciences* 439, 1907 (1992), 553–558.
- [15] David Elieser Deutsch, Adriano Barenco, and Artur Ekert. 1995. Universality in quantum computation. *Proceedings of the Royal Society of London. Series A: Mathematical and Physical Sciences* 449, 1937 (1995), 669–677. <https://doi.org/10.1098/rspa.1995.0065> arXiv:<https://royalsocietypublishing.org/doi/pdf/10.1098/rspa.1995.0065>
- [16] Cirq Developers. 2022. Cirq. (Dec 2022). <https://doi.org/10.5281/zenodo.7465577> See full list of authors on Github: <https://github.com/quantumlib/Cirq/graphs/contributors>.
- [17] Cirq Developers. 2022. Cirq. <https://doi.org/10.5281/zenodo.7465577> See full list of authors on Github: <https://github.com/quantumlib/Cirq/graphs/contributors>.
- [18] DGBJ Dieks. 1982. Communication by EPR devices. *Physics Letters A* 92, 6 (1982), 271–272.
- [19] Hassan Eldib and Chao Wang. 2014. Synthesis of masking countermeasures against side channel attacks. In *International Conference on Computer Aided Verification*. Springer, 114–130.
- [20] Edward Farhi, Jeffrey Goldstone, and Sam Gutmann. 2014. A quantum approximate optimization algorithm. *arXiv preprint arXiv:1411.4028* (2014).
- [21] Serguei Fedortchenko. 2016. A quantum teleportation experiment for undergraduate students. <https://doi.org/10.48550/ARXIV.1607.02398>
- [22] J. M. Gambetta, F. Motzoi, S. T. Merkel, and F. K. Wilhelm. 2011. Analytic control methods for high-fidelity unitary operations in a weakly nonlinear oscillator. *Phys. Rev. A* 83 (Jan 2011), 012308. Issue 1. <https://doi.org/10.1103/PhysRevA.83.012308>
- [23] Lov K. Grover. 1996. A Fast Quantum Mechanical Algorithm for Database Search. In *Proceedings of the Twenty-Eighth Annual ACM Symposium on Theory of Computing* (Philadelphia, Pennsylvania, USA) (STOC ’96). Association for Computing Machinery, New York, NY, USA, 212–219. <https://doi.org/10.1145/237814.237866>
- [24] IBM. [n.d.]. Qiskit: Elements for building a quantum future. <https://github.com/Qiskit/qiskit>.
- [25] IBM. [n.d.]. Qiskit: Solving Linear Systems of Equations using HHL. [https://qiskit.org/textbook/ch-applications/hhl\\_tutorial.html](https://qiskit.org/textbook/ch-applications/hhl_tutorial.html).
- [26] IBM Quantum. 2023. <https://quantum-computing.ibm.com/>.
- [27] Joseph T. Iosue. [n.d.]. QAOAPython: The Quantum Approximate Optimization Algorithm implemented on Cirq, ProjectQ, and Qiskit. <https://github.com/jtiosue/QAOAPython>.
- [28] Ali JavadiAbhari, Shruti Patil, Daniel Kudrow, Jeff Heckey, Alexey Lvov, Frederic T Chong, and Margaret Martonosi. 2014. ScaffCC: A framework for compilation and analysis of quantum computing programs. In *Proceedings of the 11th ACM Conference on Computing Frontiers*. 1–10.
- [29] P. Krantz, M. Kjaergaard, F. Yan, T. P. Orlando, S. Gustavsson, and W. D. Oliver. 2019. A quantum engineer’s guide to superconducting qubits. *Applied Physics Reviews* 6, 2 (2019), 021318. <https://doi.org/10.1063/1.5089550> arXiv:<https://doi.org/10.1063/1.5089550>
- [30] Ang Li, Samuel Stein, Sriram Krishnamoorthy, and James Ang. 2022. QASMBench: A Low-Level Quantum Benchmark Suite for NISQ Evaluation and Simulation. *ACM Transactions on Quantum Computing* (2022).
- [31] Jarrod R McClean, Nicholas C Rubin, Kevin J Sung, Ian D Kivlichan, Xavier Bonnet-Monroig, Yudong Cao, Chengyu Dai, E Schuyler Fried, Craig Gidney, Brendan Gimby, et al. 2020. OpenFermion: the electronic structure package for quantum computers. *Quantum Science and Technology* 5, 3 (2020), 034014.
- [32] David C. McKay, Christopher J. Wood, Sarah Sheldon, Jerry M. Chow, and Jay M. Gambetta. 2017. Efficient Z gates for quantum computing. *Phys. Rev. A* 96 (Aug 2017), 022330. Issue 2. <https://doi.org/10.1103/PhysRevA.96.022330>
- [33] Rafaele Miceli. [n.d.]. Quantum\_Walks: Qiskit code to simulate quantum walks on graphs with up to 4 nodes. [https://github.com/rafamiceli/Quantum\\_Walks](https://github.com/rafamiceli/Quantum_Walks).
- [34] Kristel Michielsen, Madita Nocon, Dennis Willsch, Fengping Jin, Thomas Lipfert, and Hans De Raedt. 2017. Benchmarking gate-based quantum computers. *Computer Physics Communications* 220 (2017), 44–55.
- [35] Microsoft Azure. 2023. Azure Quantum. <https://azure.microsoft.com/en-us/products/quantum>
- [36] Microsoft Azure Quantum. 2023. <https://azure.microsoft.com/en-us/resources/development-kit/quantum-computing>.
- [37] Andrew Moss, Elisabeth Oswald, Dan Page, and Michael Tunstall. 2012. Compiler assisted masking. In *International Workshop on Cryptographic Hardware and Embedded Systems*. Springer, 58–75.
- [38] F. Motzoi, J. M. Gambetta, P. Rebentrost, and F. K. Wilhelm. 2009. Simple Pulses for Elimination of Leakage in Weakly Nonlinear Qubits. *Phys. Rev. Lett.* 103 (Sep 2009), 110501. Issue 11. <https://doi.org/10.1103/PhysRevLett.103.110501>
- [39] James L Park. 1970. The concept of transition in quantum mechanics. *Foundations of physics* 1, 1 (1970), 23–33.

- [40] Alberto Peruzzo, Jarrod McClean, Peter Shadbolt, Man-Hong Yung, Xiao-Qi Zhou, Peter J Love, Alán Aspuru-Guzik, and Jeremy L O'brien. 2014. A variational eigenvalue solver on a photonic quantum processor. *Nature communications* 5, 1 (2014), 4213.
- [41] Emmanuel Prouff and Matthieu Rivain. 2013. Masking against side-channel attacks: A formal security proof. In *Annual International Conference on the Theory and Applications of Cryptographic Techniques*. Springer, 142–159.
- [42] Qiskit contributors. 2023. Qiskit: An Open-source Framework for Quantum Computing. <https://doi.org/10.5281/zenodo.2573505>
- [43] Qiskit Custom Gates. 2023. [https://qiskit.org/documentation/tutorials/circuits\\_advanced/05\\_pulse\\_gates.html](https://qiskit.org/documentation/tutorials/circuits_advanced/05_pulse_gates.html).
- [44] Gonçalo Sampaio. 2017. Code in QASM for quantum circuits and algorithms. <https://github.com/sampaio96/Quantum-Computing>.
- [45] Samuel A Stein, Ryan L'Abbate, Wenrui Mu, Yue Liu, Betis Baheri, Ying Mao, Guan Qiang, Ang Li, and Bo Fang. 2021. A hybrid system for learning classical data in quantum states. In *2021 IEEE International Performance, Computing, and Communications Conference (IPCCC)*. IEEE, 1–7.
- [46] Jakub Szefer. 2018. Principles of Secure Processor Architecture Design. *Synthesis Lectures on Computer Architecture* 13, 3 (2018), 1–173.
- [47] Kentaro Tamura and Yutaka Shikano. 2021. Quantum random numbers generated by a cloud superconducting quantum computer. In *International Symposium on Mathematics, Quantum Theory, and Cryptography: Proceedings of MQC 2019*. Springer Singapore, 17–37.
- [48] Joel J. Wallman and Joseph Emerson. 2016. Noise tailoring for scalable quantum computation via randomized compiling. *Phys. Rev. A* 94 (Nov 2016), 052325. Issue 5. <https://doi.org/10.1103/PhysRevA.94.052325>
- [49] Jingbo Wang, Chunga Sung, Mukund Raghothaman, and Chao Wang. 2021. Data-Driven Synthesis of Provably Sound Side Channel Analyses. In *2021 IEEE/ACM 43rd International Conference on Software Engineering (ICSE)*. IEEE, 810–822.
- [50] Jingbo Wang, Chunga Sung, and Chao Wang. 2019. Mitigating power side channels during compilation. In *Proceedings of the 2019 27th ACM Joint Meeting on European Software Engineering Conference and Symposium on the Foundations of Software Engineering*. 590–601.
- [51] Nathan Wiebe, Ashish Kapoor, and Krysta M Svore. 2014. Quantum deep learning. *arXiv preprint arXiv:1412.3489* (2014).
- [52] William K Wootters and Wojciech H Zurek. 1982. A single quantum cannot be cloned. *Nature* 299 (1982), 802–803.